PCCP

PAPER

Cite this: *Phys. Chem. Chem. Phys.*, 2015, **17**, 16483

Interaction of 4-imidazolemethanol with a copper electrode revealed by isotope-edited SERS and theoretical modeling†

Ieva Matulaitienė,[a] Eglė Pociūtė,[b] Zenonas Kuodis,[a] Olegas Eicher-Lorka[a] and Gediminas Niaura*[a]

Received 4th March 2015,
Accepted 28th May 2015

DOI: 10.1039/c5cp01290b

www.rsc.org/pccp

Adsorption of 4-imidazolemethanol (ImMeOH) on a copper electrode has been investigated by *in situ* isotope-edited (H/D and $^{63}Cu/^{65}Cu$) surface enhanced Raman spectroscopy (SERS) in aqueous solutions at physiological pH (7.0) in a potential window from −0.500 to −1.100 V. Theoretical modeling by DFT calculations at the B3LYP/6-311++G(d,p) level for light atoms and LANL2DZ with ECP for copper atoms have been employed for the interpretation of experimental data. The copper surface was modeled by a cluster of 6 atoms. It was found that the imidazole ring adopts Tautomer-I form in the adsorbed state and coordinates with the Cu surface through the N3 atom. Linear potential-dependence of ν(C4═C5) mode with the slope of (15 ± 1) cm^{-1} V^{-1} was experimentally observed. The imidazole ring mode near 1492 cm^{-1} primarily due to ν(C2–N3) + β(C2H) vibration has also showed a considerable decrease in frequency at more negative electrode potentials with the slope of (9 ± 2) cm^{-1} V^{-1}. Both modes can be used as sensitive probes for analysis of interaction of the imidazole ring with the metal surface. In agreement with experimental data theoretical modeling has predicted higher stability of surface bound Tautomer-I compared with Tautomer-II. The formation of a covalent bond between the metal and adsorbate was experimentally evidenced by metal isotopic ($^{63}Cu/^{65}Cu$) frequency shift of ν(Cu–N) mode at 222 cm^{-1}, combined with theoretical modeling of the surface complex.

Introduction

Interaction of functional groups of amino acids with metals is an important issue in the fields of biocatalysis, biosensors, and biocompatibility. The imidazole ring plays an important role in the coordination of metal ions in proteins and provides an active site for binding with metals at electrochemical interfaces.[1–4] In addition, participation of imidazole and its derivatives in corrosion prevention and modification of metal surfaces has been demonstrated.[5–9] These compounds served as useful corrosion inhibitors in the case of copper electrodes.[8–11] A relatively low toxicity of imidazole derivatives has been stressed as an important advantage for corrosion inhibition of Cu in hydrochloric and sulfuric acids.[11] To predict and control the formation of complexes at the interface, molecular level understanding the imidazole binding mode with surface and adsorption geometry is required. Surface enhanced Raman spectroscopy (SERS) is able to provide detailed information on adsorption of molecules and ions at certain metals (mainly Au, Ag, and Cu) because of submonolayer sensitivity and molecular specificity.[12–14] Importantly, SERS spectra might be collected *in situ* at potential control, because of the low interference of water scattering to the surface spectrum.[12,15–18] In addition, the low-frequency vibrational region (100–500 cm^{-1}) where important metal–adsorbate vibrational modes appear is easily accessible. These vibrational modes give direct information on the formation of surface complexes at the interface.[19–22] Anionic and neutral forms of the adsorbed imidazole ring on the Ag surface depending on the electrode potential and solution pH were detected by SERS.[23] Previous studies of adsorption of histidine amino acid and histamine onto metal surfaces have revealed the importance of carboxyl and amine functional groups in addition to ring nitrogen atoms on interaction with the surface.[24–27] Reorientation of the imidazole ring of adsorbed histamine at the Ag electrode from perpendicular to a more parallel configuration was detected as the electrode potential was switched from −0.800 to −0.500 V (*vs.* Ag/AgCl).[26] The influence of the electrode potential as well as the nature of solution anions (Cl^- and SO_4^{2-}) and pH on the coordination of histidine with a copper electrode surface was

[a] *Department of Organic Chemistry, Center for Physical Sciences and Technology, A. Gostauto 9, Vilnius, LT-01108, Lithuania. E-mail: gniaura@ktl.mii.lt; Fax: +3705 2729373; Tel: +3705 2729642*

[b] *Faculty of Chemistry, Vilnius University, Naugarduko 24, Vilnius, LT-03225, Lithuania*

† Electronic supplementary information (ESI) available: Comparison of solution Raman and SERS spectra at different concentrations (Fig. S1); SERS spectra of phosphate anions (Fig. S2); structures of Cu_6–ImMeOH–H_2O complexes (Fig. S3); calculated Mulliken atom charges (Table S1); and calculated bond lengths of complexes Cu_6–ImMeOH–H_2O (Table S2). See DOI: 10.1039/c5cp01290b

demonstrated.[25] Dissimilar adsorption structures of histidine on Au and Ag nanoparticles have been revealed by SERS.[24] In the case of an Au electrode a flat ring orientation was suggested, while the strong interaction of the carboxylate group resulted in a perpendicular ring orientation for the Ag substrate. Recently, the participation of an imidazole ring of histidine amino acid residue in bonding with a copper electrode of decapeptide neuromedin B was revealed by potential-difference SERS spectroscopy.[28]

In this work we have chosen one of the simplest imidazole derivatives, 4-imidazolemethanol (ImMeOH). It does not contain surface active or bulky functional groups, thus facilitating a direct interaction of the imidazole group with the metal. ImMeOH was used for the synthesis of imidazole ring containing compounds.[29] A copper electrode was chosen because of biologically important metal known to interact with amino acids and peptides forming complexes in aqueous solutions.[30,31] Furthermore, the understanding of binding of an imidazole ring containing derivatives to the copper surface is important for corrosion inhibition development. In this work we have studied *in situ* the electrode potential effect on the adsorption behavior of 4-imidazolemethanol at the copper electrode in buffered (pH 7.0) aqueous solution by using a SERS technique. Isotopic-edited SERS based on labile hydrogen atom substitution by deuterium and substrate ^{63}Cu exchange to ^{65}Cu was employed for the reliable interpretation of the surface spectra.

Experimental

Materials

Millipore-purified water (18 MΩ cm) was used for the preparation of solutions. Chemicals were of ACS reagent grade. ImMeOH and D_2O were purchased from Sigma-Aldrich GmbH (Germany). ^{63}CuO and ^{65}CuO were obtained from Cambridge Isotope Laboratories, Inc. (USA).

SERS and Raman measurements

The polarized Raman spectra of ImMeOH (0.5 M) in H_2O and D_2O solutions were recorded using a Raman spectrometer inVia (Renishaw) equipped with a grating containing 1800 grooves per mm and a CCD detector thermoelectrically cooled to −70 °C. The 532 nm radiation from a DPSS laser (Cobolt) was used as the excitation source. The laser power at the sample was 60 mW. Raman spectra were taken using 5×/0.12 NA objective lens (Leica). The accuracy in the measurement of the depolarization ratios (ρ) was checked with CCl_4; the ρ values for 218, 315, and 459 cm^{-1} bands were obtained to be 0.75, 0.75, and 0.008, respectively.

Near-infrared Raman and SERS spectra were recorded using Echelle type spectrometer RamanFlex 400 (PerkinElmer, Inc.) equipped with a thermoelectrically cooled (−50 °C) CCD camera and fiber-optic cable for excitation and collection of the surface-enhanced Raman scattering. The 785 nm beam of the diode laser was used as the excitation source. The 180° scattering geometry was employed. The laser power at the sample was 30 mW, and the beam was focused to a 200 μm diameter spot. The integration time was 10 s. Each spectrum was recorded by the accumulation of 30 scans yielding an overall integration time of 300 s. The Raman frequencies were calibrated using the polystyrene standard (ASTM E 1840) spectrum. Intensities were calibrated by a NIST intensity standard (SRM 2241). Experiments were conducted at 20 °C. Spectroelectrochemical measurements were carried out in a cylindrical three-electrode cell configured with a circular quartz window and a flat circular working Cu electrode of ∼5 mm in diameter that was press-fitted into a Teflon rod. The working electrode was placed at ∼3 mm from the cell window. The Pt wire and KCl-saturated Ag/AgCl electrodes were used as the counter and reference electrodes, respectively. The potential values reported below refer to this reference electrode. To eliminate the laser-induced photo- and thermo-effects, the cell, together with the electrodes, was moved linearly with respect to the laser beam at a rate of 15–25 mm s^{-1} using custom-built equipment.[20,32] Oxygen was eliminated from the solutions by continuously bubbling the ultra pure Ar gas. The solution concentration of ImMeOH in SERS studies was 10^{-4} M.

Before experiments the Cu electrode was polished with soft sandpaper (P2500) and a 0.3 μm alumina slurry (Stuers, Denmark) for refreshing the surface and sonicated in a water–ethanol mixture (1 : 1, v/v) for 10 min. Then, the electrode was transferred into the cell containing 0.02 M $CuSO_4$ with pH adjusted to 4.5 and a SERS active fresh Cu layer was electrodeposited at −0.500 V potential for 3 min.[19] The morphology of the roughened Cu electrode surface was characterized previously.[33] Isotopic experiments ^{63}Cu/^{65}Cu were performed by dissolving the required amount of ^{63}CuO and ^{65}CuO in dilute H_2SO_4 solution while heating to obtain 0.02 M $CuSO_4$ (pH 4.5) electrolytes. Subsequently, SERS active ^{63}Cu and ^{65}Cu electrodes were obtained by electrodeposition.

Frequencies and intensities of the SERS bands were determined by fitting the experimental contour with Gaussian–Lorentzian form components. The background spectrum of 0.1 M Na_2SO_4 containing 0.01 M phosphate buffer (H_2O/D_2O) was subtracted from SERS spectra. Spectral analysis was performed by using GRAMS/A1 8.0 (Thermo Scientific) software.

Theoretical modeling

All calculations were performed using Gaussian for Windows package version G03W D.01.[34] Geometry optimization and harmonic vibrational frequency calculations were accomplished with a density functional theory (DFT) method, using a B3LYP functional. Calculations were done using a 6-311++G(d, p) basis set for C, H, N, and O atoms, and LANL2DZ with ECP for Cu atoms. The cluster model used to represent the metal surface was built with fully optimized 6 copper atoms. Calculated frequencies were scaled by the relationship: $\nu' = \alpha(\nu)\cdot\nu$, where ν' and $\alpha(\nu)$ are the scaled frequency and the scaling factor, respectively. The scaling factor was defined by the following equation:[35]

$$\alpha(\nu) = 1 - (1 - \alpha^{F})\frac{\nu - \nu^{0}}{\nu^{F} - \nu^{0}}, \quad (1)$$

using the parameters: α^F = 0.97, ν^F = 4000, and ν^0 = 600. Calculated Raman scattering activities (S_j) were scaled by converting them to the Raman cross sections ($\partial\sigma/\partial\Omega$) which are

proportional to the Raman intensities and can be compared with the experimental data. The Raman scattering cross sections were calculated by using the following equation:[36,37]

$$\frac{\partial\sigma_j}{\partial\Omega} = \left(\frac{2^4\pi^4}{45}\right)\left(\frac{(\nu_0-\nu_j)^4}{1-\exp\left[\frac{-hc\nu_j}{kT}\right]}\right)\left(\frac{h}{8\pi^2 c\nu_j}\right)S_j, \qquad (2)$$

where ν_0 is the laser excitation frequency, ν_j is the vibrational frequency of the jth normal mode, and h, c and k are the universal constants. Predicted vibrational spectra were generated by using a Lorentzian function for broadening of Raman lines with 4 cm^{-1} full width at half-maximum (FWHM) values.

Results and discussion

Solution Raman spectra of ImMeOH

In neutral aqueous solutions ImMeOH may exist in two tautomeric forms (Fig. 1) depending on which of nitrogen atoms (N1 or N3) is protonated. These tautomers can be easily discriminated by Raman spectroscopy.[38,39] Fig. 2 compares parallel (∥) and perpendicularly (⊥) polarized solution Raman spectra of ImMeOH in H_2O and D_2O. The depolarization ratios ($\rho = I_\perp/I_\parallel$) of Raman bands provide information on the symmetry of the vibrations and are very useful in making the assignments of the bands. Peak positions and depolarization ratios as well as the assignment of the bands are listed in Table 1. The intense polarized band observed at 1575 and 1568 cm^{-1} in H_2O and D_2O solutions, respectively, belongs to ν(C4═C5) stretching vibrations and its position indicates that Tautomer-I dominates in aqueous solutions of ImMeOH. The low intensity shoulder detected at 1591 cm^{-1} near the 1575 cm^{-1} peak is assigned to ν(C4═C5) mode from Tautomer-II.[38,39] Based on integrated intensity ratio, A_{1575}/A_{1591}, the concentration ratio of Tautomer-I to Tautomer-II is found to be 6.1. This is considerably the higher prevalence of Tautomer-I when compared with the aqueous solution of histidine amino acid (4 times).[40] The calculated spectra of Tautomer-I of Im-CH_2-OH and deuterated by labile hydrogens ImD-CH_2-OD are also displayed in Fig. 2. In excellent agreement with experimental spectra the ν(C4═C5) bands were predicted at 1574 and 1567 cm^{-1} for natural and deuterated structures. Calculated spectra, ρ values determined from experimental data, and previously published studies on vibrational analysis of imidazole ring derivatives[38–41] were used for the assignment of the bands presented in Table 1. In the C–H stretching frequency region two pairs of bands associated with stretching vibrations of the methylene group (2888–2954 cm^{-1}) and the imidazole ring (3133–3157 cm^{-1}) are clearly visible (Fig. 2). Calculated spectra allowed a secure assignment of ν(C5–H) and ν(C2–H) modes of the imidazole ring to 3157 and 3133 cm^{-1} components of the experimental spectrum (Table 1).

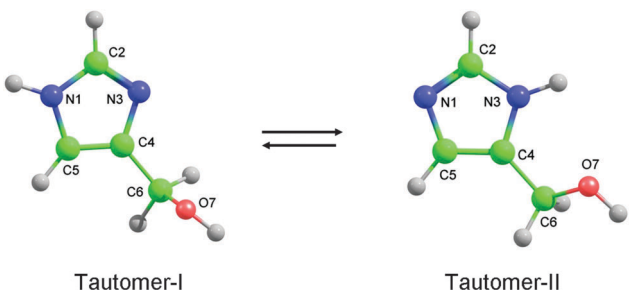

Fig. 1 Structures and atom numbering of 4-imidazolemethanol (ImMeOH) tautomers optimized at the DFT-B3LYP/6-311++G(d,p) level.

Overview of the SERS spectra of ImMeOH on the Cu electrode

Fig. 3 compares 785 nm excited solution Raman and SERS spectra of ImMeOH at 0.5 M and 10^{-4} M concentrations, respectively. No bands associated with solution ImMeOH were possible to observe at 10^{-4} M concentration (Fig. S1 in ESI†), indicating that the roughened Cu electrode used in this work support the SERS effect. Numerous changes in the peak positions, relative intensities, and widths of the bands are visible in the SERS spectrum. The intense feature visible near 937 cm^{-1} belongs to adsorbed phosphate anions.[42–44] This band usually appears in neutral or slightly alkaline phosphate buffer solution, provided that the Cu surface is sufficiently clean without amorphous carbon impurities or strongly chemisorbed organic species.[44] The peak frequency of the phosphate band downshifts and the FWHM decreases at more negative electrode potentials. SERS bands of adsorbed phosphate anions are clearly visible in the blank solution spectrum before the introduction of ImMeOH (Fig. S2, ESI†). The well-defined bands in the fingerprint spectral region (Fig. 3A) near 1107, 1279, 1345, 1491, and 1579 cm^{-1} belong to the imidazole ring vibrations of adsorbed ImMeOH. The observation of SERS bands from both phosphate species and the imidazole ring modes indicate that phosphate anions and ImMeOH coadsorbs at the Cu electrode surface. The relative intensities of the bands near 982, 1325, 1464, and 1575 cm^{-1} considerably decrease in the surface spectrum. Particularly substantial is the decrease in the relative intensity of 982 cm^{-1} mode associated mainly with the rocking vibration of the $C6H_2$ side chain group, rock($C6H_2$); this band is also coupled with in-plane deformation vibration of the imidazole ring, δ(C2N3C4) and stretching vibration of the carbon–oxygen bond, ν(C6–O7) (Table 1). The other band associated with the deformation vibration of the $C6H_2$ group appears as an intense band in the solution spectrum near 1464 cm^{-1}. The assignment of this band is confirmed by the high value of the depolarization ratio (ρ = 0.55) (Fig. 2 and Table 1). However, this band is barely visible in the SERS spectrum (Fig. 3A). It seems that the intensity of deformation and rocking modes of the side chain $C6H_2$ group is considerably attenuated in the SERS spectrum. In the C–H stretch spectral region (Fig. 3B) SERS bands broaden and shift to a lower wavenumber range. In particular, the downshift of stretching vibrational modes of the methylene group near 2889/2953 cm^{-1} is considerably higher (27/45 cm^{-1}) when compared with 3133 cm^{-1} imidazole ring ═C–H vibration (4 cm^{-1}).

Labile hydrogens H/D isotope-edited SERS spectra

To ensure accurate assignments of the bands, isotope-edited SERS experiments for labile hydrogen atoms at the imidazole ring and the OH group were performed in solutions prepared

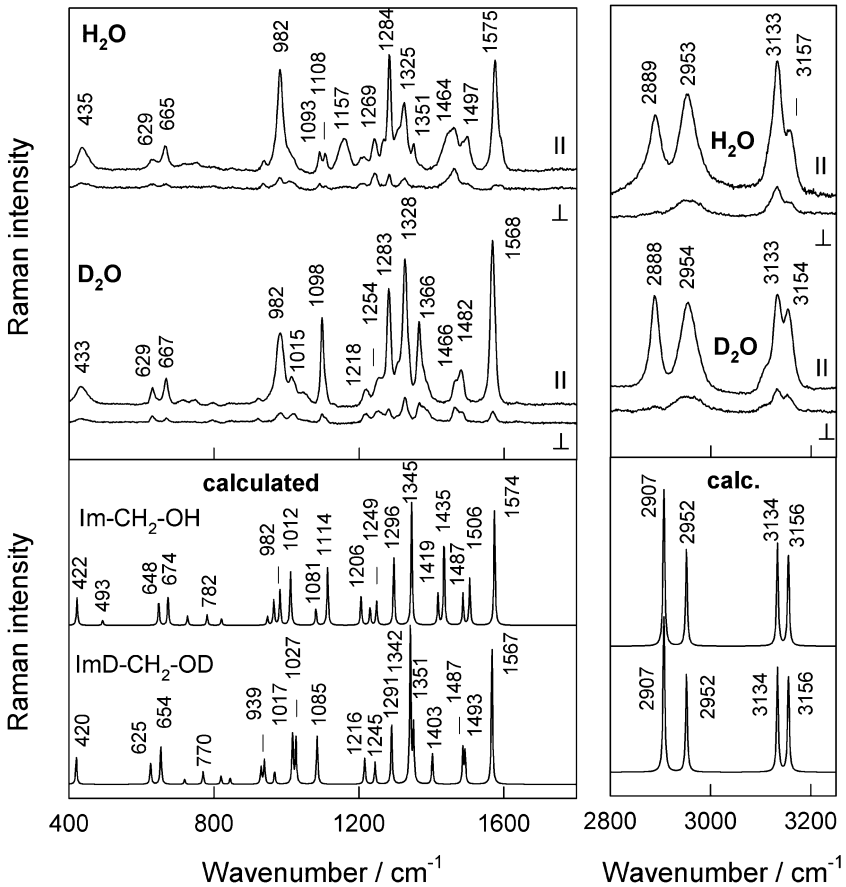

Fig. 2 Polarized (∥) and depolarized (⊥) Raman spectra in 400–1800 cm^{-1} (left panel) and 2800–3250 cm^{-1} (right panel) spectral regions of 0.5 M ImMeOH in H_2O and D_2O solutions and the calculated Raman spectrum of Im-CH_2-OH and ImD-CH_2-OD. Measurement conditions: excitation wavelength, 532 nm; laser power at the sample, 60 mW; integration time, 200 s.

with H_2O and D_2O at −1.100 V electrode potential (Fig. 4). Two well-defined bands located at 1579 and 1491 cm^{-1} clearly shift in D_2O solution to 1574 and 1486 cm^{-1}, respectively. Comparison with solution and calculated spectra allowed the assignment of these bands to ν(C4═C5) and mixed ν(C2–N3) + β(C2H) modes, respectively. Observed shifts immediately confirm that in the adsorbed state one of the imidazole ring of the nitrogen atoms is protonated. The peak at 1279 cm^{-1} shows only a slight shift and was assigned to the imidazole ring breathing mode coupled with C2–H in-plane bending vibration. It was demonstrated that the position of this band is extremely useful for the discrimination of different tautomeric forms of the imidazole ring appearing near 1282 and 1260 cm^{-1} for Tautomer-I and Tautomer-II, respectively.[38] Thus, experimental SERS data evidence that in the adsorbed state the Tautomer-I dominates. In such a structure the interaction with surface must take place through the N3 atom of the imidazole ring (Fig. 1).[40,41] The analysis of Raman spectra of metal complexes of histidine revealed an upshift of C4═C5 mode upon binding with metal cations.[41] As seen from Fig. 3 the frequency of the C4═C5 band increases in SERS spectra by 4 cm^{-1}. Such a frequency upshift value is characteristic of N3–metal coordinated complexes[41] and provides evidence that a direct interaction with the copper electrode surface takes place through the N3 site. The intensification of the band near 1328 cm^{-1} was clearly observed in the D_2O solution Raman spectrum (Fig. 2). Because, Tautomer-I prevails in aqueous solution, the observation of the similar band in the SERS spectrum of Cu electrode immersed in solution prepared with D_2O solvent (1333 cm^{-1}) confirms the dominating Tautomer-I form in the adsorbed state of ImMeOH. Finally, the intense peak in the D_2O SERS spectrum near 1103 cm^{-1} corresponds to mixed ν(N1–C2) + β(N1H) + β(C2H) mode (Table 1). The position of this band is blue-shifted by 5 cm^{-1} when compared with the solution D_2O Raman spectrum. Because of the involvement of N1H bending mode this shift might be associated with changes in hydrogen bonding interaction strength for the adsorbed molecule.

Potential dependence

Fig. 5 compares the SERS spectra of ImMeOH at selected Cu electrode potentials. It should be noted that adsorbed species are visible in the broad potential window (from −0.500 to −1.100 V). The positions of two bands located near 1579 and 1491 cm^{-1} (E = −1.100 V) are highly sensitive to the electrode potential. More quantitative analysis of the potential dependence of these bands is provided in Fig. 6. Linear dependence is observed for the ν(C4═C5) mode with a slope of (15 ± 1) $cm^{-1}\,V^{-1}$. Analysis of crystalline compounds of metal complexes with an

Table 1 Experimental and calculated wavenumbers (in cm^{-1}), depolarization ratios (ρ), and assignments of ImMeOH in solution and in the adsorbed state on Cu electrode

Raman				SERS[b]			
H_2O	D_2O	ρ[d]	Calculated[a]	H_2O	D_2O	Calc. complex[c]	Assignment
3157 m	3154 s	0.22	3156			3164	ν(C5–H)
3133 vs	3133 s	0.19	3134	3129 m	3129 m	3155	ν(C2–H)
2953 s	2954 s	0.16	2952	2908 s	2910 s	2991	$\nu_{as}(C6H_2)$
2889 s	2888 s	0.05	2907	2862 s	2864 s	2916	$\nu_s(C6H_2)$
1575 vs	1568 vs	0.04	1574	1579 s	1574 s	1584	ν(C4═C5) + ν(C4–C6) + β(C5H)
1497 m	1482 m	0.14	1506	1491 m	1486 m	1508	ν(C2–N3) + β(C2H) + ν(C2–N1) + ν(C5–N1)
1464 m	1466 w	0.55	1435			1472	$\delta(C6H_2)$
1444 sh		~0.1	1419	1445 m		1453	β(N1H) + ν(N1–C2)
1325 s	1328 vs	0.14	1345	1345 m	1333 s	1331	ν(C2–N3) + ν(N3–C4) + β(C5H)
1284 vs	1283 vs	0.10	1296	1279 vs	1276 s	1287	ν(Im) breathing + β(C2H) + ν(C4–C6)
1243 m	1218 m	0.62	1249		1210 w	1244	β(C5H) + β(C2H) + ν(C5–N1)
1157 s	1098 s	0.06	1114	1144 w	1103 s	1143	ν(N1–C2) + β(N1H) + β(C2H)
1108 m		0.15	1081	1107 m		1083	ν(C5–N1) + β(C5H)
1093 m		0.28	1012		1038 m	1041	ν(C6–O) + ν(C6–C4) + ν(C4–N3)
982 vs	982 s	0.10	982	987 w		1007	Rock($C6H_2$) + δ(C2N3C4) + ν(C6–O7)
937 w	925 w	0.68	948			942	δ(C5N1C2) + δ(C2N3C4)
665 m	667 m	0.12	674	709 s		667	γ(Im)
629 w	629 m	0.40	648	663 w		648	γ(Im)
435 m	433 m	0.21	422	444 m		432	γ(C4C6O)
322 w	322 w	0.73		313 m	311 m	332	Rock($C6H_2$) + δ(C6C4) + δ(CuN)
				222 s	222 s	242	ν(Cu–N)
				148 s	152 s	167	$\nu_s(Cu_6)$

[a] Calculated for Tautomer-I of ImMeOH in the vacuum. [b] At electrode potential −1.100 V. [c] Calculated for Tautomer-I of complex Cu_6–ImMeOH. [d] Estimated for ImMeOH in H_2O. Abbreviations: ν, stretching; δ, deformation; β, in-plane bending; γ, out-of-plane deformation; vs, very strong; s, strong; m, middle; w, weak; wag, wagging; Im, imidazole ring.

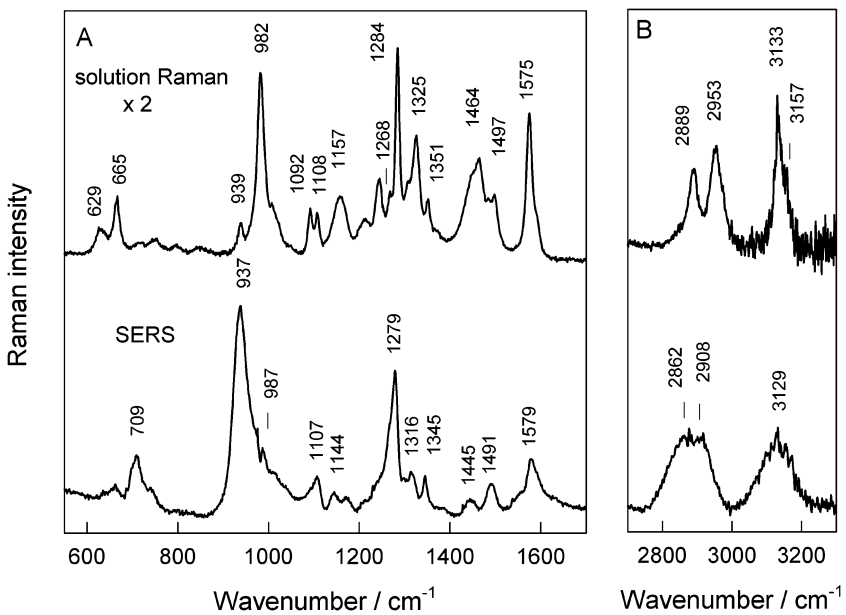

Fig. 3 Raman spectrum of 0.5 M ImMeOH aqueous solution and SERS spectrum from the Cu electrode in 10^{-4} M ImMeOH aqueous solution containing 0.1 M Na_2SO_4 and 0.01 M phosphate buffer (pH 7.0) at −1.100 V potential in the fingeprint (A) and C–H stretching frequency (B) spectral regions. The background spectrum of water and buffer was subtracted from solution and SERS spectra, respectively. Measurement conditions: excitation wavelength, 785 nm; laser power at the sample, 30 mW; integration time, 300 s.

imidazole ring has revealed a correlation between the ν(C4═C5) band frequency and the C4═C5 bond length;[41] higher frequency corresponds to a shorter bond. In the case of N1–H/N3–metal complexes (Tautomers-I) the 1573, 1580, and 1588 cm^{-1} wavenumbers correspond to 137.9, 136.9, and 135.4 pm bond lengths.[41] Thus, an observed decrease in the peak frequency at a more negative electrode potential reveal the lengthening of the C4═C5 bond because of a decrease in the interaction strength with the metal surface.

The peak position of the second lower frequency band also shifts to lower wavenumbers at more negative electrode potentials (Fig. 6b). However, the slope was found to be considerably smaller

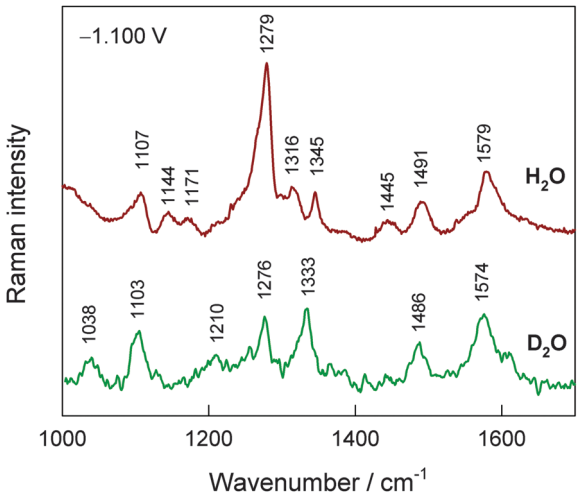

Fig. 4 SERS spectra of ImMeOH adsorbed on the Cu electrode at −1.100 V potential in solutions prepared from H_2O and D_2O. The Raman spectrum of buffer was subtracted. Measurement conditions: 0.1 M Na_2SO_4 solution containing 0.01 M phosphate buffer (pH 7.0) and 10^{-4} M of ImMeOH; excitation wavelength, 785 nm; laser power at the sample, 30 mW; integration time, 300 s.

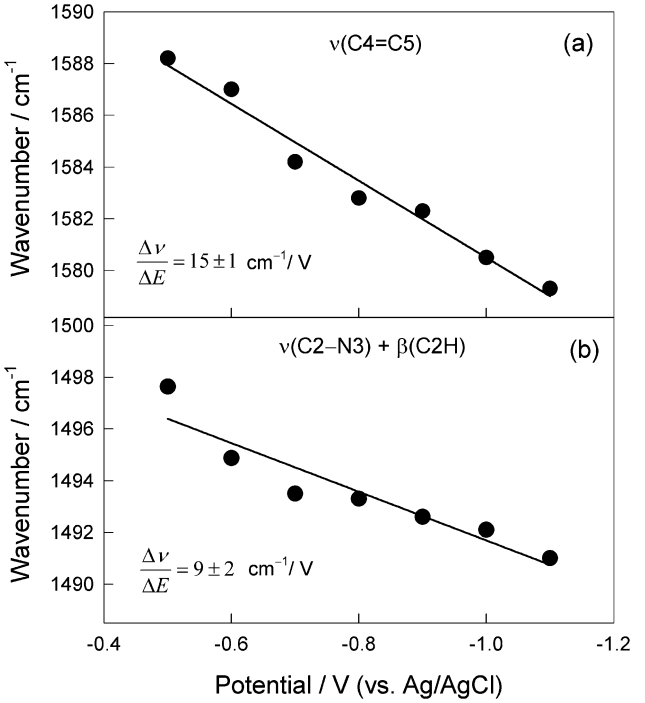

Fig. 6 Potential dependence of the SERS peak wavenumbers for (a) ν(C4═C5) and (b) ν(C2–N3) + β(C2H) vibrational modes.

(9 ± 2 cm^{-1} V^{-1}). This mode involves large contribution from C2–N3 stretching and C2–H in-plane bending vibrations. Because for Tautomer-I the N3 atom of the imidazole ring is involved in bonding with the metal, potential-induced changes in the interaction with the surface might modulate this mode frequency. Importantly, in the case of Tautomer-II the main contributions for the experimentally observed band near 1493 cm^{-1} in the solution

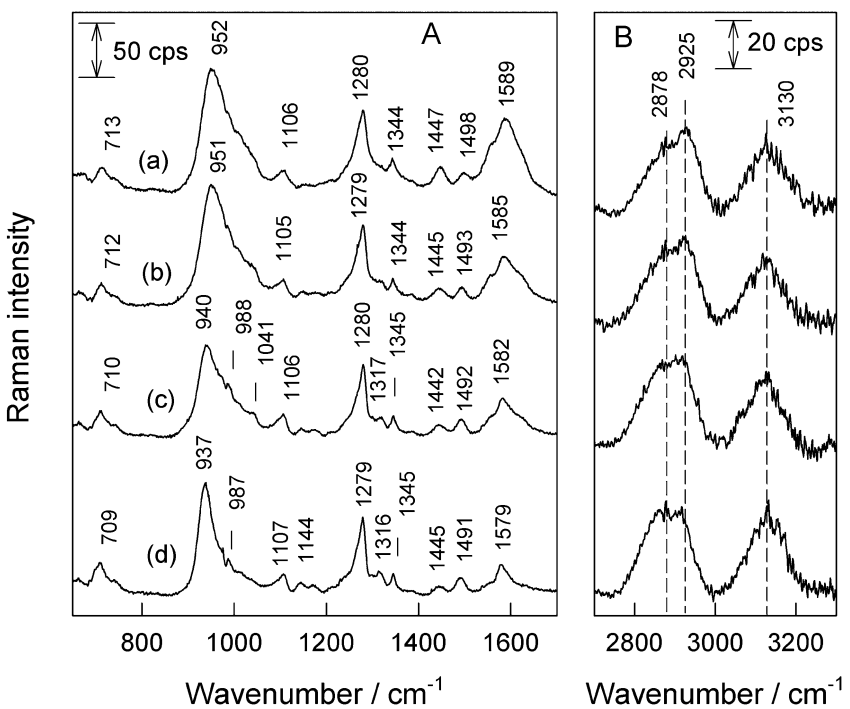

Fig. 5 SERS spectra of ImMeOH adsorbed on the Cu electrode at −0.500 (a), −0.700 (b), −0.900 (c), and −1.100 V (d) electrode potentials in the fingerprint (A) and C–H stretching frequency (B) spectral regions. The Raman spectrum of buffer was subtracted. Measurement conditions: 0.1 M Na_2SO_4 solution containing 0.01 M phosphate buffer (pH 7.0) and 10^{-4} M of ImMeOH; excitation wavelength, 785 nm; laser power at the sample, 30 mW; integration time, 300 s.

spectrum consists of ν(N1–C2) + β(C2H).[38] Thus, this mode must be the coordination sensitive band, because it involves bonding with the metal atom N1. Indeed, the appearance of the new band at higher frequencies (1503 cm^{-1}) was clearly visible in the experimental Raman spectra of Cu(II)–(βAla–His) or Zn(II)–(zinc finger) complexes in an N3–H/N1–metal coordination state.[41]

The positions of the high frequency C–H stretching bands of the methylene group are considerably downshifted in SERS spectra (2878–2925 cm^{-1}) (Fig. 5) when compared with the solution Raman spectrum (2889 and 2953 cm^{-1}) (Fig. 3). The effect is even better pronounced at more negative electrode potentials (Fig. 7A). This indicates surface induced restriction to vibrations because of the contact of the imidazole ring and methylene group with Cu atoms. For more detailed analysis of C–H stretching bands the potential-difference spectrum was constructed (Fig. 7A). Broad positively going feature with a maximum near 2844 cm^{-1} is visible in the difference spectrum. Previously, we have identified an unusually low frequency C–H stretching band of methylene groups from bifunctional thiols adsorbed at Ag and Au electrodes associated with the direct interaction of methylene groups with the metal surface.[45] Similar soft methylene stretching bands were observed by infrared reflection absorption spectroscopy studies of adsorption of alkyl chain containing molecules on metal surfaces.[46,47] Importantly, such a low frequency band was also observed in the SERS spectra of adsorbed peptides at the Ag electrode at sufficiently negative potential values.[48] Thus, the presented data indicate that the methylene group is in contact with the electrode surface upon adsorption of ImMeOH at copper electrode at more negative electrode potentials. Such contact with the surface might be responsible for the attenuation of relative intensities of deformation scissoring and rocking modes of the $C6H_2$ group in SERS spectra. The soft mode intensity dependence on electrode potential (Fig. 7B) indicates that the reorientation of molecules so that CH_2 groups approach the Cu electrode surface takes place in the potential region from −0.60 to −0.90 V. It should be noted that C–H stretching bands considerably broaden upon adsorption of ImMeOH on the Cu electrode. Thus, the width of the methylene group C–H stretching bands determined as FWHM increases from 32 (2889 cm^{-1} band) and 41 cm^{-1} (2953 cm^{-1} band) to 109 (2878 cm^{-1} band) and 57 cm^{-1} (2925 cm^{-1} band) for adsorbed species at −0.5 V potential, respectively. Considering the imidazole ring =C–H stretching modes, only one broad feature near 3130 cm^{-1} was visible in the surface spectrum, while two clear bands at 3133 and 3157 cm^{-1} exhibits a solution Raman spectrum. It should be noted that deuteration of the imidazole ring induces a slight shift of 3157 cm^{-1} component to 3154 cm^{-1} for ImMeOH in D_2O solvent (Fig. 2). FWHM of the imidazole ring =C–H stretching mode broadens from 26 cm^{-1} (3133 cm^{-1} band) to 111 cm^{-1} for adsorbed species. Such considerable broadening of the =C–H band confirms the involvement of the imidazole ring in bonding with the electrode surface.

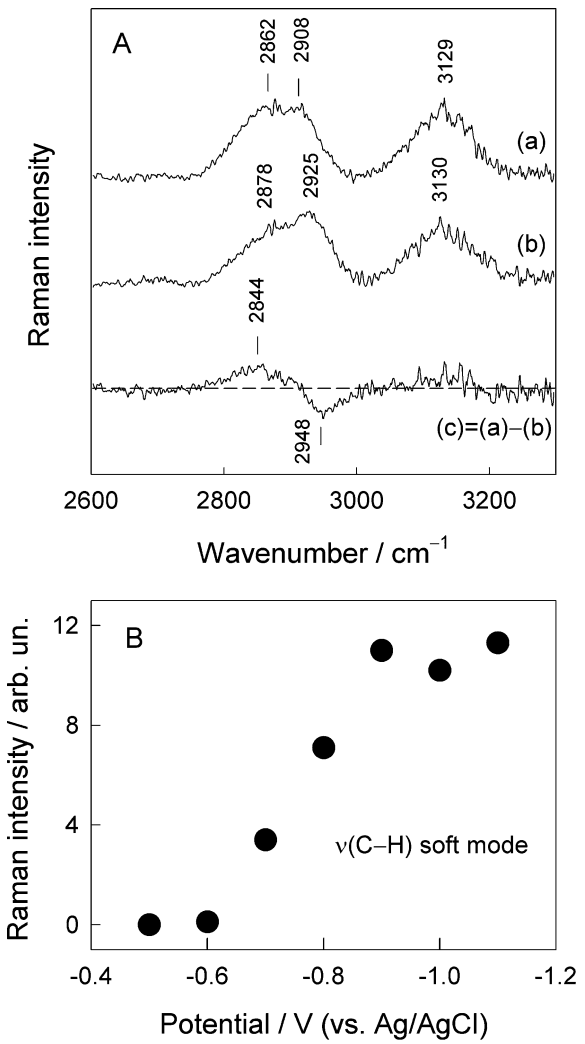

Fig. 7 (A) SERS spectra in the C–H stretching spectral region of ImMeOH adsorbed on the Cu electrode at (a) −1.100 V and (b) −0.500 V. The difference spectrum (c) is also shown. (B) Dependence of intensity of C–H soft mode near 2844 cm^{-1} from methylene groups on electrode potential. Soft band was obtained by subtraction the spectrum at −0.500 V from that obtained at given potential. Measurements conditions: 0.1 M Na_2SO_4 solution containing 0.01 M phosphate buffer (pH 7.0) and 10^{-4} M of ImMeOH; excitation wavelength, 785 nm; laser power at the sample, 30 mW; integration time, 300 s.

Important information on orientation of the imidazole ring with respect to the copper electrode surface might be derived from the analysis of relative intensities in solution Raman and SERS spectra. The SERS surface selection rule suggests that the most intense bands are associated with the vibrational modes with polarizability tensor components oriented perpendicular to the metal surface.[49,50] In the case of compounds with a planar structure, particularly useful is the analysis of a relative magnitude of the =C–H stretching band.[51,52] Since for aromatic molecules the polarizability tensor lies predominantly along the =C–H axis, observation of an intense band indicates a predominant vertical orientation of the molecule at the metal surface.[52] We have estimated a relative surface enhancement factor (SEF) by comparing the integrated intensity ratio for =C–H stretching vibrational mode of the imidazole ring in SERS and solution spectra [$SEF_{(=C-H)} = (A_{SERS}/A_{solution})_{=C-H}$]. Intensities were normalized to breathing vibrational mode of the imidazole ring

observed at 1284 and 1279 cm^{-1} in solution and surface spectra, respectively (Fig. 3). At electrode potential −1.100 V the $SEF_{(=C-H)}$ value was found to be 1.75, indicating a tilted orientation of the imidazole ring plane. A shift of the electrode potential to −0.500 V results in a decrease of $SEF_{(=C-H)}$ to 1.35. Thus, it can be suggested that the angle between the ring plane and the surface normal increases as potential becomes less negative.

$^{63}Cu/^{65}Cu$ metal isotope-edited SERS spectra in the low frequency region

Direct information on bonding of adsorbates with a metal surface might be extracted by the SERS technique from the analysis of a low-frequency spectral region.[21,22] Fig. 8 shows SERS spectra in the 120 to 800 cm^{-1} range at selected electrode potentials. Three bands located near 149, 222, and 313 cm^{-1} (−1.100 V) might be associated with deformation and stretching vibration of the Cu–N bond.[53] The position of the former two bands slightly varies (within 4 cm^{-1}) with electrode potential, while the frequency of the latter band more clearly decreases at a more negative electrode potential. The ν(Cu–N) band was detected near 310 cm^{-1} by Raman spectroscopic analysis of the Cu(II)–histamine complex.[54] For a precise assignment of metal–adsorbate vibrational modes we have performed metal isotope-edited SERS experiments (Fig. 9). The blue shift of the band located near 219 cm^{-1} was clearly visible when the ^{65}Cu layer was changed to ^{63}Cu. An exact isotope-induced frequency shift [$k = \nu(^{63}Cu–N) - \nu(^{65}Cu–N)$] was determined from the analysis of second derivatives of the corresponding SERS spectra and it was found to be 2.6 ± 0.5 cm^{-1}. The shoulder near 258 cm^{-1} observable in the SERS spectrum became clearly visible in the second derivative spectrum. No frequency shift was detected for this mode in the wavenumber limit of ±0.5 cm^{-1}. Thus, this vibrational mode does not involve the motion of a Cu atom and probably is associated with deformation vibration of adsorbate. It was not possible to determine precisely the shift of the broad low frequency feature near 149 cm^{-1}. However, we can conclude that this band remains unshifted in a frequency limit of ±2 cm^{-1}.

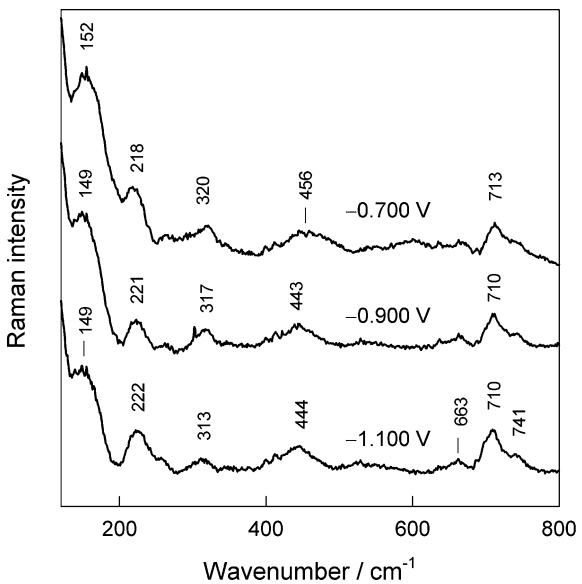

Fig. 8 Potential dependence of SERS spectra of ImMeOH adsorbed on the Cu electrode in the low frequency spectral region. Measurement conditions: 0.1 M Na_2SO_4 solution containing 0.01 M phosphate buffer (pH 7.0) and 10^{-4} M of ImMeOH; excitation wavelength, 785 nm; laser power at the sample, 30 mW; integration time, 300 s.

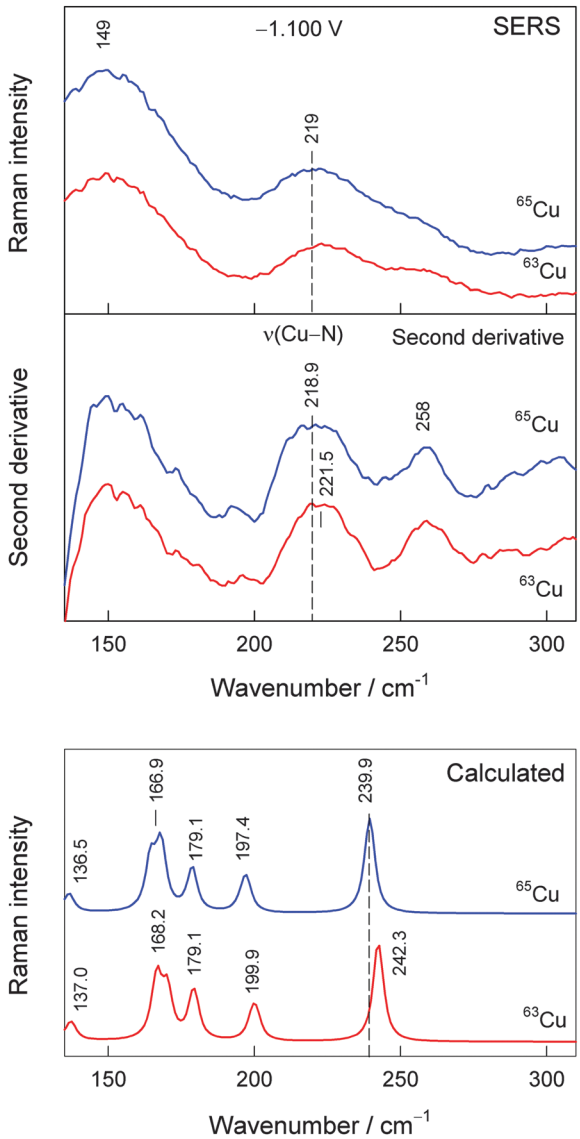

Fig. 9 Isotopic $^{63}Cu/^{65}Cu$ edited SERS spectra of ImMeOH adsorbed on a Cu electrode at −1.100 V in the metal–adsorbate spectral region with corresponding second derivative SERS spectra (multiplied by −1) (upper panel), and calculated low-frequency Raman spectra of $^{65}Cu_6$–ImMeOH and $^{63}Cu_6$–ImMeOH complexes (bottom panel).

Theoretical modeling of the surface complex

In order to confirm the assignments of the bands and get insight into the bonding of the imidazole ring with copper surface theoretical modeling of Cu_6–ImMeOH complexes for Tautomer-I and Tautomer-II was performed. Structures with fully optimized metal clusters ($^{65}Cu/^{63}Cu$) were considered.

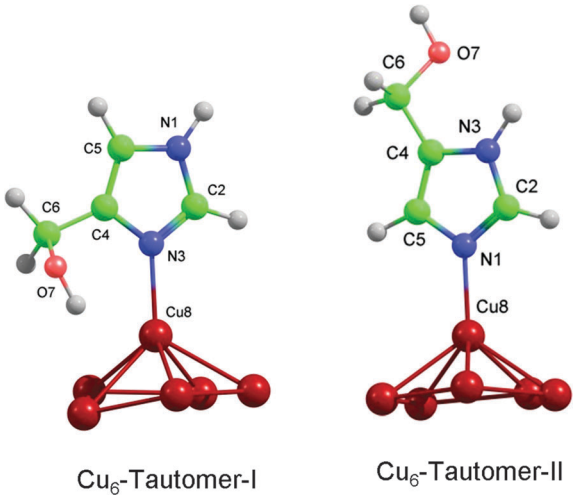

Fig. 10 Structures of Cu_6–ImMeOH complexes optimized at the DFT-B3LYP/6-311++G(d,p) level for C, H, N, and O atoms, and LANL2DZ with ECP for Cu atoms.

Fig. 10 shows the optimized geometries of Cu_6–ImMeOH complexes. The calculated energies revealed that the Tautomer-I complex structure is more stable (by 7.7 kcal mol^{-1}) than the Tautomer-II. This theoretical prediction is in accord with experimental SERS observation of prevalence of Tautomer-I in the adsorbed state. The main difference between these complexes is that the weak interaction of the OH group takes place in the Tautomer-I case with one of the Cu atom. Such an interaction is clearly visible by the downshifted ν(O–H) mode frequency from 3689 cm^{-1} (Tautomer-II) to 3515 cm^{-1} (Tautomer-I). The bond lengths for different conformers are compared in Table 2. The O7–H bond length increases by 0.90 pm upon bonding of Tautomer-I with Cu_6 cluster, while the length of this bond slightly decreases (0.12 pm) in the case of Tautomer-II. Other bonds of the imidazole ring are affected to a higher extent for this structure as well. To account for the bonding with metal cluster induced perturbations in the structure of adsorbate, we have introduced the average bond change:

$$\delta = n^{-1} \sum_{n} |\Delta_i|, \qquad (3)$$

where Δ_i is the lengthening (shortening) of the particular i bond because of bonding of the molecule with the metal cluster and n is the number of considered bonds in the adsorbate. For bonded Tautomer-I and Tautomer-II the δ value was found to be 0.84 and 0.42 pm, respectively. Thus, the interaction of Tautomer-I with copper cluster results in considerably higher structural perturbations of the molecule. The lengths of the bonds adjusted to the N atom, which is involved in the bonding with copper cluster (C2–N3 and C4–N3 for Tautomer-I and C5–N1 and C2–N1 for Tautomer-II) increase upon chemisorption. However, the length of the C4═C5 bond decreases by 0.48 pm upon formation of surface complex in the case of Tautomer-I (Table 2). Correspondingly, the frequency of ν(C4═C5) mode increases. Such adsorption induced blue shift is consistent with experimentally observed SERS spectra (Table 1). It should be noted that calculations suggest a smaller decrease in the bond length (less frequency shift) upon formation of a surface complex with Tautomer-II (Table 2).

The calculated Cu–N bond length (203.3 pm) for surface bound imidazole ring of Tautomer-I is slightly higher compared with crystalline metal ion complexes of histidine and histidine-containing peptides observed experimentally (196.2–201.9 pm).[41] Calculations predict Cu–N stretching vibrational mode at 242.3 and 239.9 cm^{-1} for $^{63}Cu_6$–ImMeOH and $^{65}Cu_6$–ImMeOH complexes, respectively (Fig. 9). A metal isotopic frequency shift for model surface complexes (k = 2.4 cm^{-1}) coincides very well with an experimentally observed value (k = 2.6 cm^{-1}), confirming the assignment of this band to the Cu–N stretching vibrational mode. Calculations suggest that the experimentally observed band near 313 cm^{-1} is associated mainly with a rocking vibration of the $C6H_2$ group with some contribution from the δ(C6C4) in-plane and δ(CuN) vibrations; no isotopic frequency shift was detected for this mode. Other lower frequency bands exhibiting a clear downshift (199.9 cm^{-1}/197.4 cm^{-1} and 168.2 cm^{-1}/166.9 cm^{-1}) upon $^{63}Cu/^{65}Cu$ exchange are associated mainly with stretching and deformation vibrations of the metal cluster. Thus, an experimentally observed band near 149 cm^{-1} might be tentatively assigned to the stretching vibration of electrode copper atoms.

To investigate the changes in the electronic structure of ImMeOH, the Mulliken charges on atoms of adsorbate before and after the surface complex formation was analyzed (Table S1, ESI†). Before bonding the N3/N1 (Tautomer-I/Tautomer-II) atoms had the largest excess electronic population (~0.3–0.4 e) of the imidazole ring, indicating the nucleophilic nature of these centers in their interaction with a metal surface. As can be seen from the

Table 2 Calculated bond lengths (pm) of Tautomer-I and -II of ImMeOH (Fig. 1) and model complexes Cu_6–ImMeOH of surface bound Tautomer-I and -II (Fig. 10)

	Tautomer-I			Tautomer-II		
Bond	Free	Surface-bound complex	Difference	Free	Surface-bound complex	Difference
C4═C5	137.03	136.55	0.48	137.01	136.84	0.17
C5–N1	137.49	137.85	−0.36	137.61	138.07	−0.46
C2–N1	136.48	135.23	1.25	131.10	131.87	−0.77
C2–N3	130.88	131.65	−0.77	136.33	135.59	0.74
C4–N3	137.98	138.52	−0.54	137.82	137.98	−0.16
C4–C6	148.85	149.66	−0.81	148.50	149.08	−0.58
C6–O7	143.70	142.11	1.59	143.55	143.19	0.36
O7–H	96.35	97.25	−0.90	96.34	96.22	0.12
Cu–N		203.32			203.54	

charge difference of atoms, $\Delta q_j = q_j(\text{complex}) - q_j(\text{free})$ (for particular j atom), bonding of the molecule with Cu_6 cluster results in pronounced charge redistribution. First of all, the negative charge on bonded N3/N1 (Tautomer-I/Tautomer-II) atoms considerably decreases (by ~0.31–0.45 e), while the relative negative charge on C4/C5 atoms, which are close to the bonded nitrogen atom significantly increases (by ~0.43–0.47 e). Secondly, in the case of Tautomer-I the noticeable electron density decrease was characteristic of the H13 atom of the C6–O7H13 moiety indicating the participation of the hydroxyl group in the interaction with the surface. Such charge redistribution results in the lengthening of the O7–H bond and the downshift of corresponding calculated stretching frequency (Table 2). Comparison of net charges for adsorbed different conformers revealed 0.111 electron charge transfer from molecule to the metal cluster in the case of Tautomer-I, while only 0.007 electron charge transfer was obtained for Tautomer-II (Table S1, ESI†).

Since the studied compound is able to form hydrogen bonds, the surface complexes with an added explicit water molecule were considered (Fig. S3, ESI†). In the case of Tautomer-I the formation of a chemical bond between water molecule and copper atom was observed, while for Tautomer-II, the water molecule was found to be in the solution phase. Optimized structures revealed the formation of a hydrogen bond between the oxygen atom O7 of adsorbed Tautomer-I and the hydrogen atom of water molecule (O7···HOH). For Tautomer-II, formation of the (O7)H···OH_2 hydrogen bond was estimated. Surprisingly, the addition of a water molecule induced minor changes in the geometry of surface complexes. Comparison of calculated energies revealed that surface complex Cu_6–Tautomer-I–H_2O (N3–Cu bonded) with an explicit water molecule is more stable by 7.78 kcal mol^{-1} when compared with Cu_6–Tautomer-II–H_2O (N1–Cu bonded) surface complex. Analysis of water-induced changes in the structure of adsorbed Cu_6–Tautomer-I–H_2O indicates slight lengthening of chemical bonds except the N3–Cu bond (Table S2, ESI†). The average perturbation of chemical bonds (δ) was found to be 0.50 pm. In the case of the Cu_6–Tautomer-II–H_2O structure, the water-induced changes in the structure of ImMeOH are less pronounced (δ = 0.36 pm). Importantly, in both cases the interaction of water with adsorbed ImMeOH slightly decreases the nitrogen–copper bond length (increases interaction strength). Experimentally adsorbed water molecules have not been detected by the SERS method in this work. It is well-known that special conditions are required for SERS observation of interfacial water.[55,56]

Conclusions

The imidazole ring is a key functional group in metal-coordinating proteins and peptides. The present study provides a detailed insight into the vibrational properties of one of the simplest imidazole derivatives, 4-imidazolemethanol (ImMeOH), adsorbed on a copper electrode surface in neutral aqueous solution. Stable isotope-edited (ImMeOH/ImDMeOD and $^{63}Cu/^{65}Cu$) SERS and theoretical modeling at the DFT-B3LYP/6-311++G(d,p) level for light atoms and LANL2DZ with ECP for copper atoms were employed to probe the potential-dependent adsorption behavior of the imidazole derivative. The adsorption complex was modeled by 6 copper atoms, Cu_6–ImMeOH. Coadsorption of phosphate anions and ImMeOH in a wide potential region has been evidenced from SERS spectra. Two imidazole ring high frequency stretching bands located near 1580 [ν(C4=C5)] and 1492 cm^{-1} [ν(C2–N3) + β(C2H)] have demonstrated a considerable downward frequency shift at more negative electrode potentials indicating the sensitivity of these modes to binding of the imidazole ring with the copper surface. The appearance of the ''soft'' C–H stretching feature near 2844 cm^{-1} has indicated the contact of the methylene group with the metal surface upon adsorption of ImMeOH on the Cu electrode at more negative electrode potentials. Experimental spectra and theoretical modeling both suggested that the most stable form of the adsorbed molecule is Tautomer-I and the imidazole ring N3 atom is a primary binding site of copper. The metal–adsorbate vibrational mode has been clearly identified in metal isotope-edited ($^{63}Cu/^{65}Cu$) SERS spectrum near 222 cm^{-1}. This assignment was confirmed by the theoretical modeling of $^{63}Cu_6$–ImMeOH and $^{65}Cu_6$–ImMeOH complexes. The results presented in this work demonstrate the utility of metal ($^{63}Cu/^{65}Cu$) isotope-edited SERS as a probe of metal–adsorbate interactions.

Acknowledgements

This work was supported by the Research Council of Lithuania (Contract No. MIP-104/2011 HISRAM).

References

1 H. Takeuchi, *Biopolymers*, 2003, **72**, 305–317.
2 V. Feyer, O. Plekan, N. Tsud, V. Cháb, V. Matolín and K. C. Prince, *Langmuir*, 2010, **26**, 8606–8613.
3 T. Miura, K. Suzuki, N. Kohata and H. Takeuchi, *Biochemistry*, 2000, **39**, 7024–7031.
4 T. Miura, A. Hori-I, H. Mototani and H. Takeuchi, *Biochemistry*, 1999, **38**, 11560–11569.
5 D. A. Carter and J. E. Pemberton, *Langmuir*, 1992, **8**, 1218–1225.
6 R. Holze, *Electrochim. Acta*, 1993, **38**, 947–956.
7 G. Xue, Q. Dai and S. Jiang, *J. Am. Chem. Soc.*, 1998, **110**, 2393–2395.
8 R. Gašparac, C. R. Martin, E. Stupnišek-Lisac and Z. Mandic, *J. Electrochem. Soc.*, 2000, **147**, 991–998.
9 H. Otmačić and E. Stupnišek-Lisac, *Electrochim. Acta*, 2003, **48**, 985–991.
10 R. Subramanian and V. Lakshminarayanan, *Corros. Sci.*, 2002, **44**, 535–554.
11 E. Stupnišek-Lisac, A. L. Bozic and I. Cafuk, *Corrosion*, 1998, **54**, 713–720.
12 P. L. Stiles, J. A. Dieringer, N. C. Shah and R. P. Van Duyne, *Annu. Rev. Anal. Chem.*, 2008, **1**, 601–626.

13 K. Kneipp, H. Kneipp, I. Itzkan, R. R. Dasari and M. S. Feld, *J. Phys.: Condens. Matter*, 2002, **14**, R597–R624.
14 A. E. Aliaga, H. Ahumada, K. Sepulveda, J. S. Gomez-Jeria, C. Garrido, B. E. Weiss-López and M. M. Campos-Vallette, *J. Phys. Chem. C*, 2011, **115**, 3982–3989.
15 I. Matulaitiene, Z. Kuodis, O. Eicher-Lorka and G. Niaura, *J. Electroanal. Chem.*, 2013, **700**, 77–85.
16 I. Matulaitiene, J. Barkauskas, R. Trusovas, G. Raciukaitis, R. Mazeikiene, O. Eicher-Lorka and G. Niaura, *Chem. Phys. Lett.*, 2013, **590**, 141–145.
17 A. M. Ricci, N. Tognalli, E. Llave, C. Vericat, L. P. M. D. Leo, F. J. Williams, D. Scherlis, R. Salvarezza and E. J. Calvo, *Phys. Chem. Chem. Phys.*, 2011, **13**, 5336–5345.
18 B. Wrzosek, J. Cukras and J. Bukowska, *J. Raman Spectrosc.*, 2012, **43**, 1010–1017.
19 G. Niaura and A. Malinauskas, *Chem. Phys. Lett.*, 1993, **207**, 455–460.
20 A. Bulovas, N. Dirvianskyte, Z. Talaikyte, G. Niaura, S. Valentukonyte, E. Butkus and V. Razumas, *J. Electroanal. Chem.*, 2006, **591**, 175–188.
21 P. Gao and M. J. Weaver, *J. Phys. Chem.*, 1986, **90**, 4057–4063.
22 G. Niaura and R. Jakubenas, *J. Electroanal. Chem.*, 2001, **510**, 50–58.
23 J. Bukowska, A. Kudelski and K. Jackowska, *J. Electroanal. Chem.*, 1991, **309**, 251–261.
24 J. K. Lim, Y. Kim, S. Y. Lee and S. W. Joo, *Spectrochim. Acta, Part A*, 2008, **69**, 286–289.
25 S. Martusevicius, G. Niaura, Z. Talaikyte and V. Razumas, *Vib. Spectrosc.*, 1996, **10**, 271–280.
26 K. L. Davis, M. L. McGlashen and M. D. Morris, *Langmuir*, 1992, **8**, 1654–1658.
27 T. Deckert-Gaudig and V. Deckert, *J. Raman Spectrosc.*, 2009, **40**, 1446–1451.
28 I. Ignatjev, E. Podstawka-Proniewicz, G. Niaura, J. R. Lombardi and L. M. Proniewicz, *J. Phys. Chem. B*, 2011, **115**, 10525–10536.
29 S. DaninosZeghal, A. AlMourabit, A. Ahond, C. Poupat and P. Potier, *Tetrahedron*, 1997, **53**, 7605–7614.
30 B. Liedberg, C. Carlsson and I. Lundström, *J. Colloid Interface Sci.*, 1987, **120**, 64–75.
31 S. M. Barlow, K. J. Kitching, S. Haq and N. V. Richardson, *Surf. Sci.*, 1998, **401**, 322–335.
32 G. Niaura, A. K. Gaigalas and V. L. Vilker, *J. Raman Spectrosc.*, 1997, **28**, 1009–1011.
33 E. Proniewicz, I. Ignatjev, G. Niaura, D. Sobolewski, A. Prahl and L. M. Proniewicz, *J. Raman Spectrosc.*, 2013, **44**, 1096–1104.
34 M. J. Frisch, G. W. Trucks, H. B. Schlegel, G. E. Scuseria, M. A. Robb, J. R. Cheeseman, J. A. Montgomery Jr., T. Vreven, K. N. Kudin, J. C. Burant, J. M. Millam, S. S. Iyengar, J. Tomasi, V. Barone, B. Mennucci, M. Cossi, G. Scalmani, N. Rega, G. A. Petersson, H. Nakatsuji, M. Hada, M. Ehara, K. Toyota, R. Fukada, J. Hasegawa, M. Ishida, T. Nakajima, Y. Honda, O. Kitao, H. Nakai, M. Klene, X. Li, J. E. Know, H. P. Hratchian, J. B. Cross, C. Adamo, J. Jaramillo, R. Gomperts, R. E. Stratmann, O. Yazyev, A. J. Austin, R. Cammi, C. Pomelli, J. W. Ochterski, P. Y. Ayala, K. Morokuma, G. A. Voth, P. Salvador, J. J. Dannenburg, V. G. Zakrzewski, S. Dapprich, A. D. Daniels, M. C. Strain, O. Farkas, D. K. Malick, A. D. Rabuck, K. Raghavachari, J. B. Foresman, J. V. Ortiz, A. Liashenko, P. Piskorz, I. Komaromi, R. L. Martin, D. J. Fox, T. Keith, M. A. Al-Laham, C. Y. Peng, A. Nanayakkara, M. Challacombe, P. M. W. Gill, B. Johnson, W. Chen, M. W. Wong, C. Gonzalez and J. A. Pople, *Gaussian 03, Revision D.01*, Gaussian, Inc., Wallingford, CT, 2004.
35 L. Riauba, G. Niaura, O. Eicher-Lorka and E. Butkus, *J. Phys. Chem. A*, 2006, **110**, 13394–13404.
36 P. L. Polavarapu, *J. Phys. Chem.*, 1990, **94**, 8106–8112.
37 G. A. Guirgis, P. Klaboe, S. Shen, D. L. Powell, A. Gruodis, V. Aleksa, C. J. Nielsen, J. Tao, C. Zheng and J. R. Durig, *J. Raman Spectrosc.*, 2003, **34**, 322–336.
38 A. Toyama, K. Ono, S. Hashimoto and H. Takeuchi, *J. Phys. Chem. A*, 2002, **106**, 3403–3412.
39 J. G. Mesu, T. Visser, F. Soulimani and B. M. Weckhuysen, *Vib. Spectrosc.*, 2005, **39**, 114–125.
40 A. Torreggiani, G. Fini and G. Bottura, *J. Mol. Struct.*, 2001, **565–566**, 341–346.
41 T. Miura, T. Satoh, A. Hori-I and H. Takeuchi, *J. Raman Spectrosc.*, 1998, **29**, 41–47.
42 G. Niaura, A. K. Gaigalas and V. L. Vilker, *J. Phys. Chem. B*, 1997, **101**, 9250–9262.
43 E. Podstawka-Proniewicz, G. Niaura and L. M. Proniewicz, *J. Phys. Chem. B*, 2010, **114**, 5117–5124.
44 I. Ignatjev, E. Proniewicz, L. M. Proniewicz and G. Niaura, *Phys. Chem. Chem. Phys.*, 2013, **15**, 807–815.
45 I. Razmute-Razme, Z. Kuodis, O. Eicher-Lorka and G. Niaura, *Phys. Chem. Chem. Phys.*, 2010, **12**, 4564–4568.
46 Y. Zhou, R. Valiokas and B. Liedberg, *Langmuir*, 2004, **20**, 6206–6215.
47 K. A. Fosser, J. H. Kang, R. G. Nuzzo and C. H. Woll, *J. Chem. Phys.*, 2007, **126**, 194707.
48 E. Podstawka, G. Niaura and L. M. Proniewicz, *J. Phys. Chem. B*, 2010, **114**, 1010–1029.
49 J. A. Creighton, *Surf. Sci.*, 1983, **124**, 209–219.
50 A. Kudelski, *Vib. Spectrosc.*, 2005, **39**, 200–213.
51 M. Moskovits and J. S. Suh, *J. Phys. Chem.*, 1988, **92**, 6327–6329.
52 X. Gao, J. P. Davies and M. J. Weaver, *J. Phys. Chem.*, 1990, **94**, 6858–6864.
53 B. Xerri, J. P. Flament, H. Petitjean, C. Berhomieu and D. Berthomieu, *J. Phys. Chem. B*, 2009, **113**, 15119–15127.
54 A. Torreggiani, A. D. Esposti, M. Tamba, G. Marconi and G. Fini, *J. Raman Spectrosc.*, 2006, **37**, 291–298.
55 G. Niaura, *Electrochim. Acta*, 2000, **45**, 3507–3519.
56 J. F. Li, Y. F. Huang, S. Duan, R. Pang, D. Y. Wu, B. Ren, X. Xu and Z. Q. Tian, *Phys. Chem. Chem. Phys.*, 2010, **12**, 2493–2502.